AD-A042 407 JOHN CARROLL UNIV CLEVELAND OHIO DEPT OF PHYSICS F/G 20/14
EFFECTS OF DIFFRACTION ON STRESS PULSE PROPAGATION.(U)
JUL 77 M R LAYTON, E F CAROME, H D DARDY N00014-75-C-0247
UNCLASSIFIED PH-77-1 NL

| OF |
AD
A042407

END
DATE FILMED
8-77
DDC

OFFICE OF NAVAL RESEARCH

Contract N00014-75-C-0247

PROJECT NR-384-309

12

TECHNICAL REPORT

PH 77-1

EFFECTS OF DIFFRACTION ON STRESS PULSE PROPAGATION

By

M. R. Layton, E. F. Carome, H. D. Dardy, and J. A. Bucaro

July 20, 1977

DEPARTMENT OF PHYSICS
JOHN CARROLL UNIVERSITY
Cleveland, Ohio 44118

Unclassified

SECURITY CLASSIFICATION OF THIS PAGE (When Data Entered)

REPORT DOCUMENTATION PAGE		READ INSTRUCTIONS BEFORE COMPLETING FORM
1. REPORT NUMBER	2. GOVT ACCESSION NO.	3. RECIPIENT'S CATALOG NUMBER
4. TITLE (and Subtitle) (6) Effects of Diffraction on Stress Pulse Propagation,		5. TYPE OF REPORT & PERIOD COVERED (9) Technical Report.
		6. PERFORMING ORG. REPORT NUMBER (14) PH-77-1
7. AUTHOR(s) (10) M. R. Layton, E. F. Carome, H. D. Dardy and J. A. Bucaro		8. CONTRACT OR GRANT NUMBER(s) (15) N00014-75-C-0247
9. PERFORMING ORGANIZATION NAME AND ADDRESS Department of Physics John Carroll University Cleveland, Ohio 44118		10. PROGRAM ELEMENT, PROJECT, TASK AREA & WORK UNIT NUMBERS NR 384-309
11. CONTROLLING OFFICE NAME AND ADDRESS (11) 20 Office of Naval Research Arlington, Virginia 22217		12. REPORT DATE July 28, 1977 13. NUMBER OF PAGES 40
14. MONITORING AGENCY NAME & ADDRESS(if different from Controlling Office) (12) 45 p.		15. SECURITY CLASS. (of this report) Unclassified 15a. DECLASSIFICATION/DOWNGRADING SCHEDULE

16. DISTRIBUTION STATEMENT (of this Report)

Approved for public release; distribution is unlimited

17. DISTRIBUTION STATEMENT (of the abstract entered in Block 20, if different from Report)

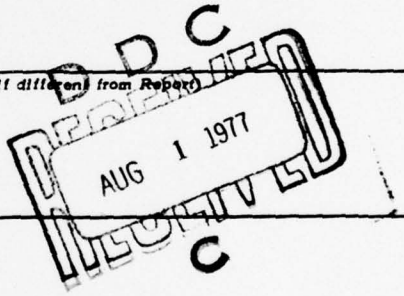

18. SUPPLEMENTARY NOTES

19. KEY WORDS (Continue on reverse side if necessary and identify by block number)

Acoustic Impulse
Acoustic Diffraction
Impulse Propagation

20. ABSTRACT (Continue on reverse side if necessary and identify by block number)

Investigations have been made of the effect of diffraction on the propagation of acoustic impulses in water. Gaussian shaped pressure pulses were obtained by applying 0.2 μsec wide voltage pulses to thick piezoelectric plates that act as piston sources. Acoustic probe techniques were used to examine in detail the resulting pressure pulses. These are strongly affected by diffraction phenomena and, because of the transient nature of the process, special care must be taken in interpreting the →next page

DD FORM 1 JAN 73 1473 EDITION OF 1 NOV 65 IS OBSOLETE
S/N 0102-LF-014-6601

Unclassified

SECURITY CLASSIFICATION OF THIS PAGE (When Data Entered)

191 675

observed data. Comparisons between experimental and theoretical time and space pressure profiles are presented.

OFFICE OF NAVAL RESEARCH

Contract N00014-75-C-0247

PROJECT NR-384-309

TECHNICAL REPORT

PH-77-1

EFFECTS OF DIFFRACTION ON STRESS PULSE PROPAGATION

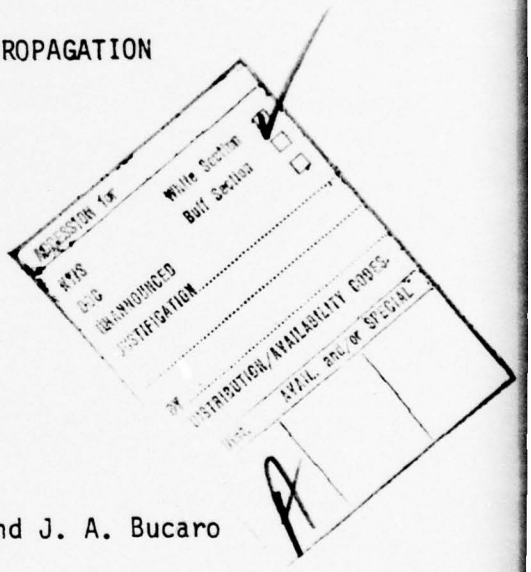

By

M. R. Layton, E. F. Carome, H. D. Dardy, and J. A. Bucaro

July 20, 1977

DEPARTMENT OF PHYSICS
JOHN CARROLL UNIVERSITY
Cleveland, Ohio 44118

TABLE OF CONTENTS

EFFECTS OF DIFFRACTION ON STRESS PULSE PROPAGATION

M. R. Layton[+] and E. F. Carome

John Carroll University

Cleveland, OH 44118

and

H. D. Dardy and J. A. Bucaro

Naval Research Laboratory

Washington, D.C. 20375

ABSTRACT

Investigations have been made of the effect of diffraction on the propagation of acoustic impulses in water. Gaussian shaped pressure pulses were obtained by applying 0.2 μsec wide voltage pulses to thick piezoelectric plates that act as piston sources. Acoustic probe techniques were used to examine in detail the resulting pressure pulses. These are strongly affected by diffraction phenomena and, because of the transient nature of the process, special care must be taken in interpreting the observed data. Comparisons between experimental and theoretical time and space pressure profiles are presented.

I. INTRODUCTION

A number of workers[1-5] have considered the use of short duration ($\sim$0.1 μsec) pressure pulses in studies of acoustic attenuation, dispersion, and scattering phenomena. Just as with continuous wave and pulsed sinusoid wave generation with sources of finite size, diffraction effects play an important role in determining the transient radiation field. Because of the less familiar nature of impulse propagation phenomena such effects, at first glance at least, may appear to differ substantially from the sinusoidal cases and some confusion has occurred in interpreting experimental results.[6] Since impulse techniques have applications in several research areas of current interest it is worthwhile to review briefly impulse generation and propagation processes, and to present relevant results of a recently completed experimental investigation of impulse diffraction phenomena.[7]

II. GENERATION OF STRESS PULSES

There are a number of techniques currently available for generating acoustic impulses. It is possible, for example, to produce large amplitude pressure transients by using Q-spoiled laser beams to impulsively heat liquid or solid targets.[8] With this technique it is possible to generate conveniently spherical, cylindrical, and plane pulses of duration less than 0.1 μsec. These have been used to examine the scattering of sound from solid objects submerged in water where their high temporal and spatial resolution has been useful in identifying the various waves that arise in

this process.

One disadvantage of using laser induced impulses is that their repetition rate is quite low and one must frequently employ "single shot" techniques. In the present study, therefore, we have employed a piezoelectric element as the sound source. This may be pulsed at a repetition rate of the order of 1 Khz, thus greatly simplifying the measurements. Typically we have used a thick, circular piezoelectric plate, of lead zirconate-lead titanate ceramic, air backed and mounted in a brass baffle plate, as indicated in Fig 1. When a Gaussian shaped voltage pulse is applied to such a plate, similarly shaped stress pulses are launched in both directions from each face of the transducer.[1] If the electrical polarity is such that the length ℓ increases, a compressional pulse is launched into the water from the right hand face and dilatational pulses are launched into the transducer from both its left and right faces. These latter two pulses propagate back and forth through the transducer and are partially transmitted into the water each time they strike the right face.

Thus in the water, for each voltage pulse applied to the source, we obtain a series of Gaussian shaped pressure pulses. As we discuss in greater detail in later sections, spatially these are defined by planes parallel to the source and are of constant amplitude over an area approximating that of the source. The temporal width of each pulse is approximately that of the applied electrical pulse, and they are separated by the travel time through the transducer, e.g., 6 microseconds for a 2.54 cm thick transducer. These may be looked on as the direct signals produced by the transducer.

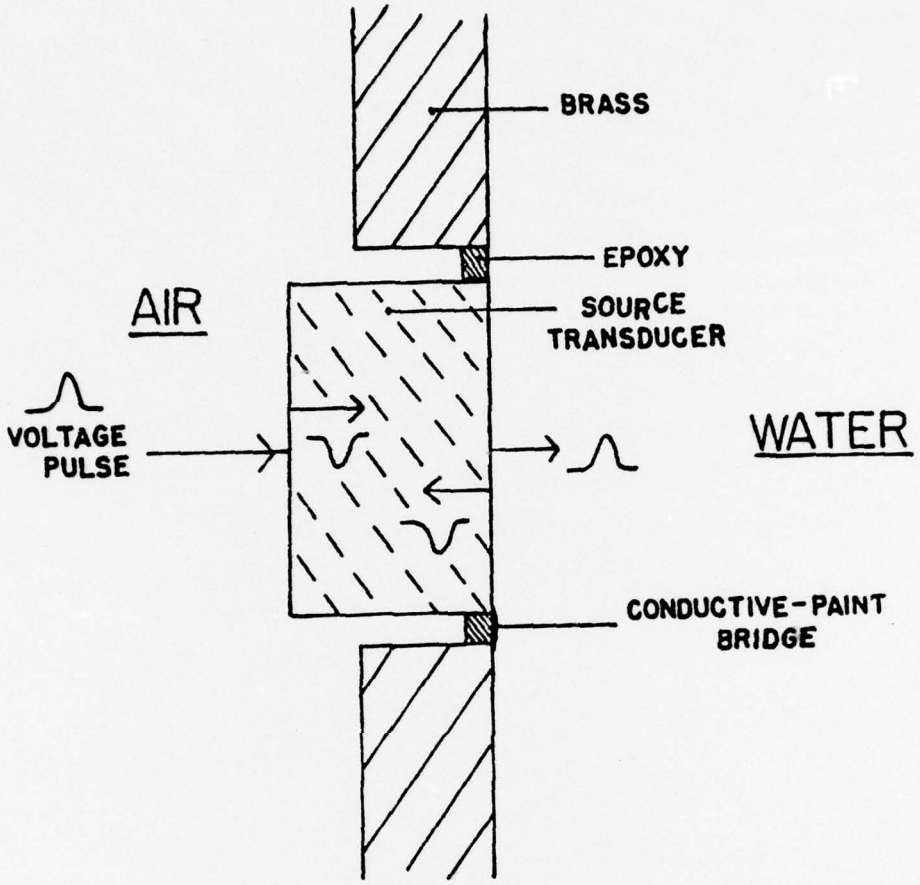

Figure 1. Cross-sectional view of the source transducer and baffle, indicating the three acoustic pulses launched for each applied voltage pulse.

III. DISCUSSION OF EFFECTIVE RING SOURCE RADIATION

In addition to these plane pressure fronts, however, there are secondary wavefronts that arise because of diffraction effects and it is these latter waves that are of specific interest in this paper. They have been considered theoretically by various authors[9-11] and we have observed them in earlier experimental studies.[2] It is convenient in the analysis to subdivide the water half space into two separate volumes. The first is the semi-infinite cylinder, the base of which is the face of the source; the second is the remaining volume of water. We refer to points in the former region as points "inside the source perimeter", and those in the latter region as points "outside".

Referring to Fig 2, assuming that the source face moves like a piston with velocity U(t), it has been shown[9] that the pressure at any point M_1 inside the perimeter a distance z from the source is given by:

$$P_{M_1}(t) = \rho v\, U[t - z/v] - \frac{\rho v}{2\pi} \int_0^{2\pi} U\left[t - \frac{R(\theta)}{v}\right] d\theta \,. \qquad (1)$$

Here $R(\theta)$ is the distance to M_1 from a particular point on the periphery of the source, and ρ and v are the density and sound velocity of water, respectively. Careful note should be taken of how the angle θ is defined in this figure. The first term in Eq (1) is the plane wave discussed above and the second represents a wave of opposite polarity from an effective ring source lying along the source perimeter. Note that temporally the plane wave contribution is independent of z and any changes in the resultant pressure

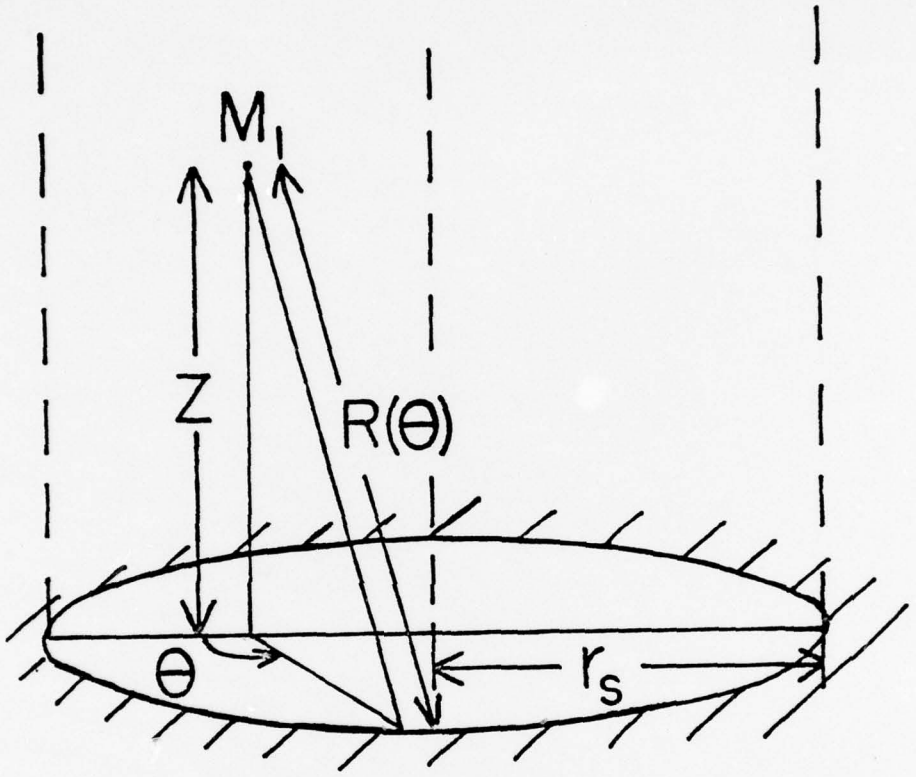

Figure 2. Sketch defining various parameters for an observation point inside the source perimeter.

field are due entirely to the way the ring source contribution varies as the observation point is changed. Cross-sectional views of the sound field at three different z separations, showing the plane wavefront and the diffracted wavefront, are shown in Fig 3 for a 1.91 cm radius source.

For a situation of experimental interest, we have calculated the pressure as a function of time for various observation points. The parameters chosen are for a source of radius r_s = 1.91 cm, excited by a Gaussian shaped voltage pulse $E(t) = E_o e^{-(t/\tau)^2}$, with τ equal to 0.1 μsec. Computed pressure versus time curves are shown in Fig 4 for observation points lying on the piston axis, at distances z from the source ranging from 5 to 100 cm. The plane wave component is centered in all cases at a time t = z/v. The first indication that the source is finite occurs with the arrival of an opposite polarity Gaussian shaped signal from the perimeter, centered at time $t = (z^2 + r_s^2)^{1/2}$. This is the mirror image of the plane wave pulse since, referring to Fig 2 and Eq (1), $R(\theta)$ remains constant as θ varies from 0 to 2π so that the contributions from all the elements of the ring source arrive simultaneously. As is evident in Fig 4, for large z values the two pulses overlap and begin to cancel.

In Fig 5 pressure versus time curves are shown for the case of observation points offset from the axis of the source by one-half the source radius. The plane wave pulse is centered, as it was previously, at t = z/v. Now, however, the delay times for the waves from the various elements of the boundary range from $t = [z^2 + (r_s - 1/2r_s)^2]^{1/2}/v$ to $t = [z^2 + (r_s + 1/2r_s)^2]^{1/2}/v$. The resulting ring source pulse is thus broadened, and the contributions to it from each element of the boundary are effectively weighted by the

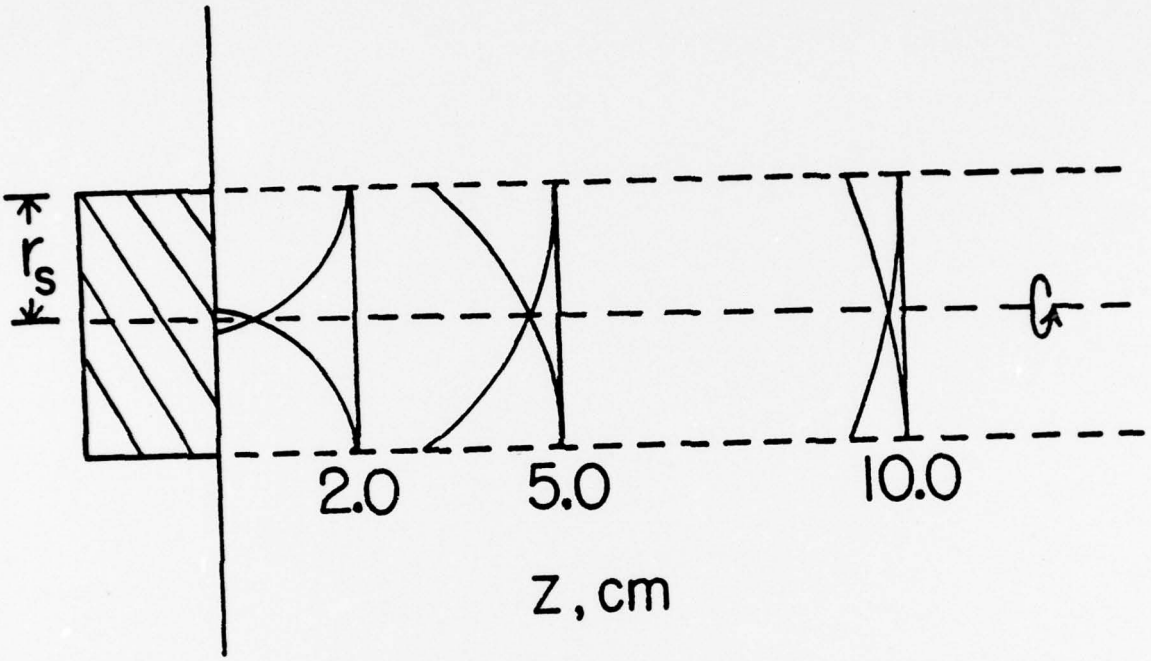

Figure 3. Sketch of the acoustic field in a single plane that intersects the transducer axis, showing the plane wave and ring source wavefronts at three different z values, for the case of a 1.91 cm radius source. The entire field is generated by rotating this figure about its axis.

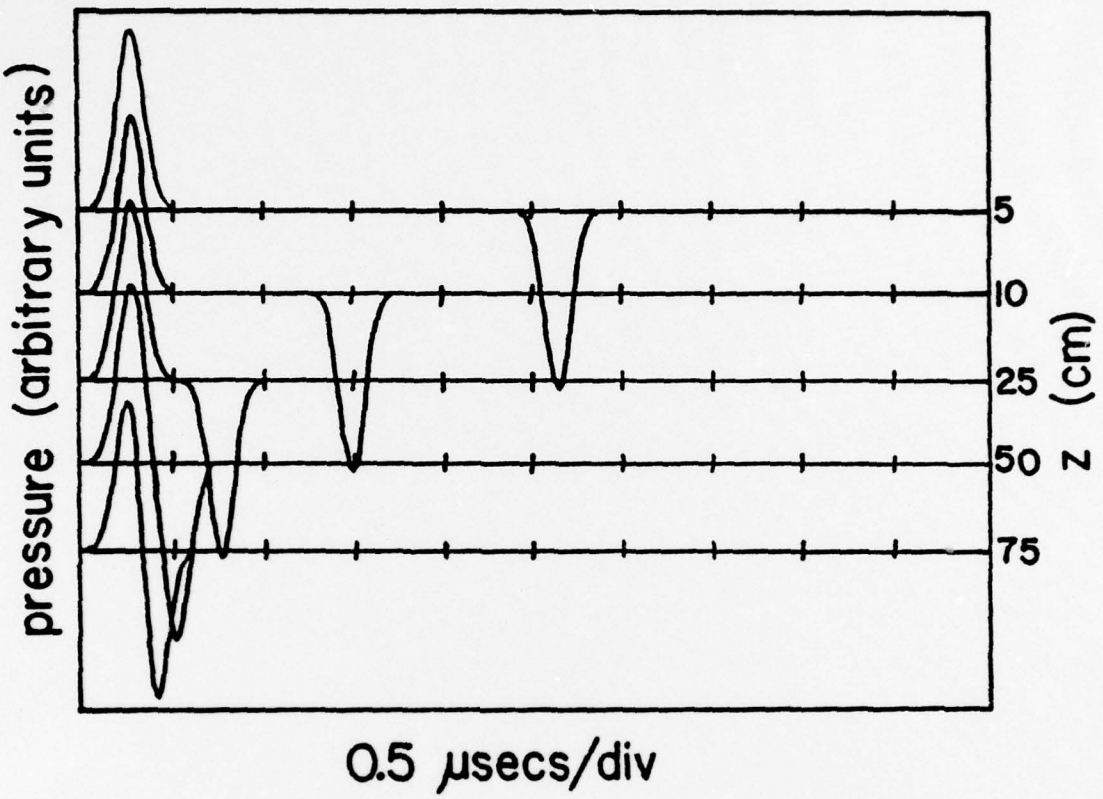

Figure 4. Calculated pressure versus time curves for observation points situated on the axis of a 1.91 cm radius piston, at five different values of z. Here the plane wave impulse at each value of z is centered at t = z/v.

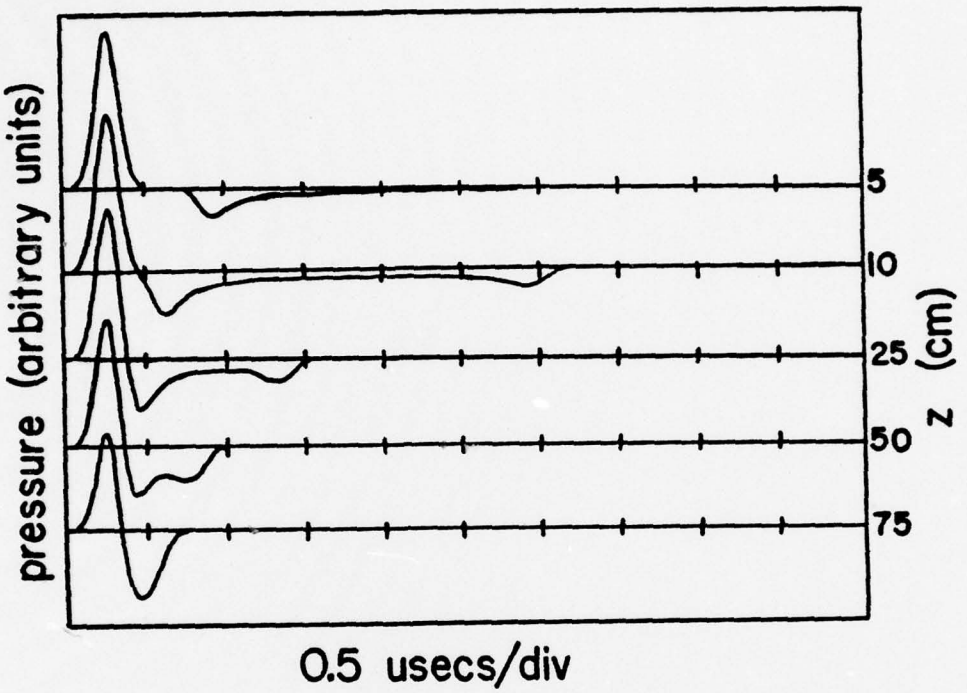

Figure 5. Calculated pressure versus time curves, for observation points offset 0.95 cm = 1/2 r_s from the axis of a 1.91 cm radius piston at five different values of z. Here the plane wave impulse at each value of z is centered at t = z/v.

behavior of $d\theta$ in Eq (1) as one integrates around the source perimeter.

The results for a point offset one source radius from the axis are shown in Fig 6. The plane wave signal and the opposite polarity contribution from the closest ring element both peak at $t = z/v$, while the signal from the farthest ring element is centered at $t = [z^2 + (2r_s)^2]^{1/2}/v$. The ring element contributions are strongly weighted by the behavior of $d\theta$, which is large near $\theta = 0$ but decays rapidly at θ goes to π. Since the initial contributions from the boundary overlap the plane wave pulse, a decrease in the positive polarity pulse amplitude is apparent when the observation point is near the edge of the source.

Next, consider an observation point M_2 lying outside the source perimeter, as indicated in Fig 7. In this region the pressure is given by:[9]

$$P_{M_2}(t) = \frac{\rho v}{2\pi}\left[2\int_0^{\theta_{max}} U\left[t = \frac{R_1(\theta)}{v}\right] d\theta - 2\int_0^{\theta_{max}} U\left[t - \frac{R_2(\theta)}{v}\right] d\theta\right], \quad (2)$$

where $R_1(\theta)$ and $R_2(\theta)$ are distances to M_2 from the two different elements of the source perimeter corresponding to a particular value of the angle θ. The pressure, then, can be considered to be due entirely to a ring source situated on the piston boundary, radiating a positive contribution from the nearer portion of the periphery and a negative contribution from the farther portion. Explicit calculations do indicate that Eqs. (1) and (2) yield identical results for observation points on the cylindrical surface separating the "inside" and "outside" regions. In Figs. 8 and 9 calculated pressure versus time profiles are shown for points offset from the axis 1.25

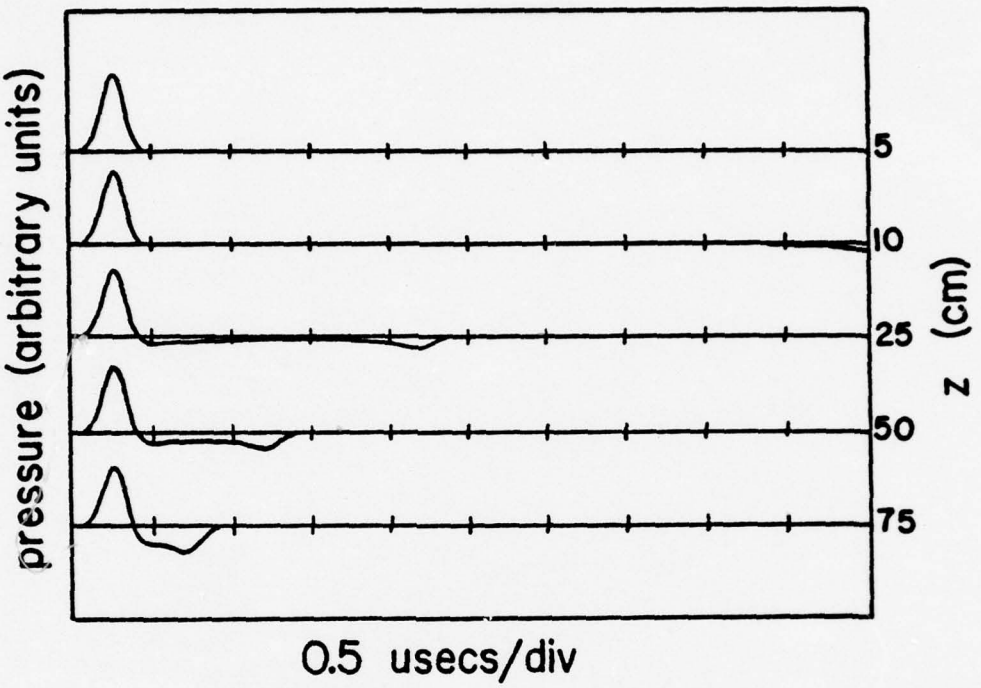

Figure 6. Calculated pressure versus time curves, for a point of observation offset 1.91 cm = r_s from the piston axis. Again, the plane wave impulse at each value of z is centeres at t = z/v.

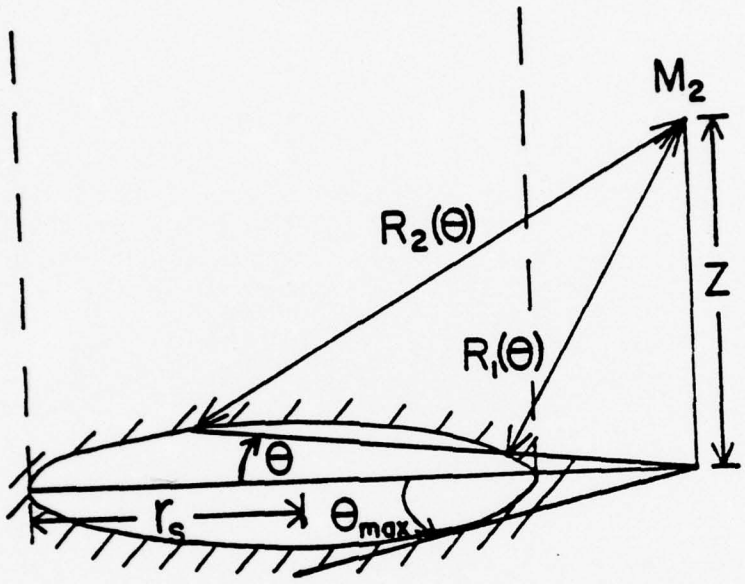

Figure 7. Sketch defining various parameters for an observation point outside the source perimeter.

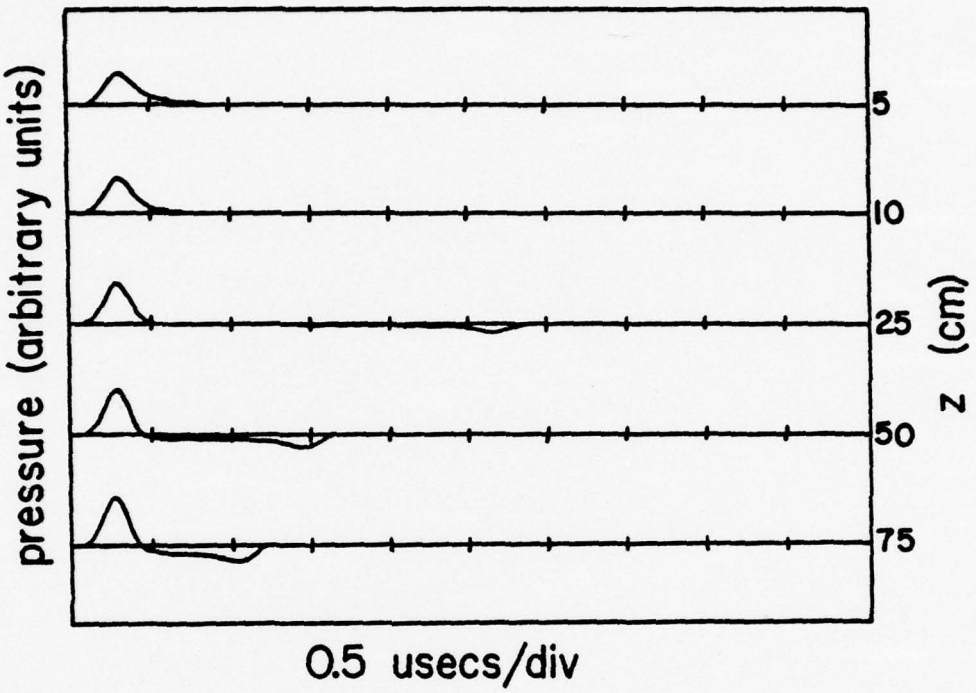

Figure 8. Calculated pressure versus time curves, for a point of observation offset 2.39 cm = 1.25 r_s from the piston axis.

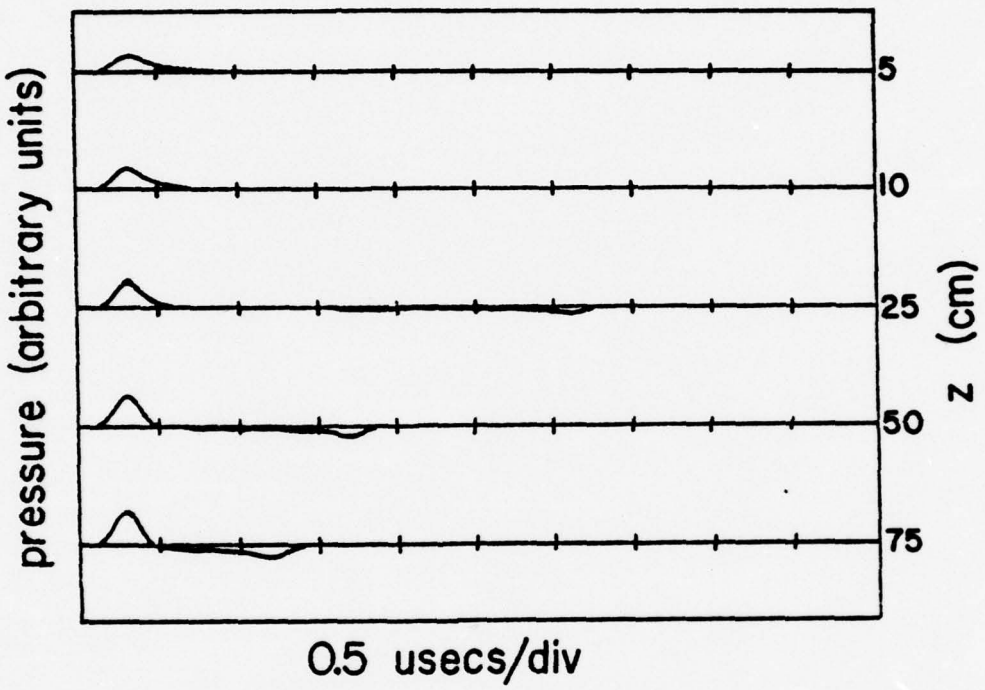

Figure 9. Calculated pressure versus time curves, for a point of observation offset 2.87 cm = 1.50 r_s from the piston axis.

and 1.5 times the source radius, respectively. The initial ring element contribution is centered at a time $t = [z^2 + [r_o - r_s]^2]^{1/2}/v$ while the final contribution is centered at a time $t = [z^2 + (r_o + r_s)^2]^{1/2}/v$. The effect of increasing z is the same as it is for points inside the source boundary: i.e., the compression of the "tail" and the approach in time of the positive and negative portions of the observed pressure variations. It is interesting to note that the predicted initial peak increases in amplitude for a particular offset as z increases over the range of z considered here.

In most experimental situations a finite diameter cylindrical receiving transducer is employed. In this case the transducer output is proportional to the space integral of the point pressure over its face. Such computations have been made for a variety of source-receiver configurations. To simplify matters, the source and receiver axes were assumed to be aligned coaxially. The calculated time variation of the integrated pressure over the face of a receiving transducer of radius $r_r = 0.32$ cm is shown in Fig 10. As in the previous calculation the source radius r_r was 1.91 cm and the applied Gaussian pulse had a half width of 0.1 μsec. The plane wave pulse arrives at all points on the disc face at the same instant of time, $t = z/v$. The contributions from the ring source which first reach the outer edge of the receiving disc, centered at $t = [z^2 + (r_s - r_r)^2]^{1/2}/v$, reach the opposite edge of the disc at $t = [z^2 + (r_s + r_r)^2]^{1/2}/v$. Again, as z increases, the ring source pulse is compressed in time, and approaches more closely the plane wave pulse. Eventually, the two begin to overlap and cancel. In Figs. 11 and 12, integrated pressure versus time curves are shown for receivers of radius $r_r = 0.64$ cm and $r_r = 0.95$ cm, respectively. The

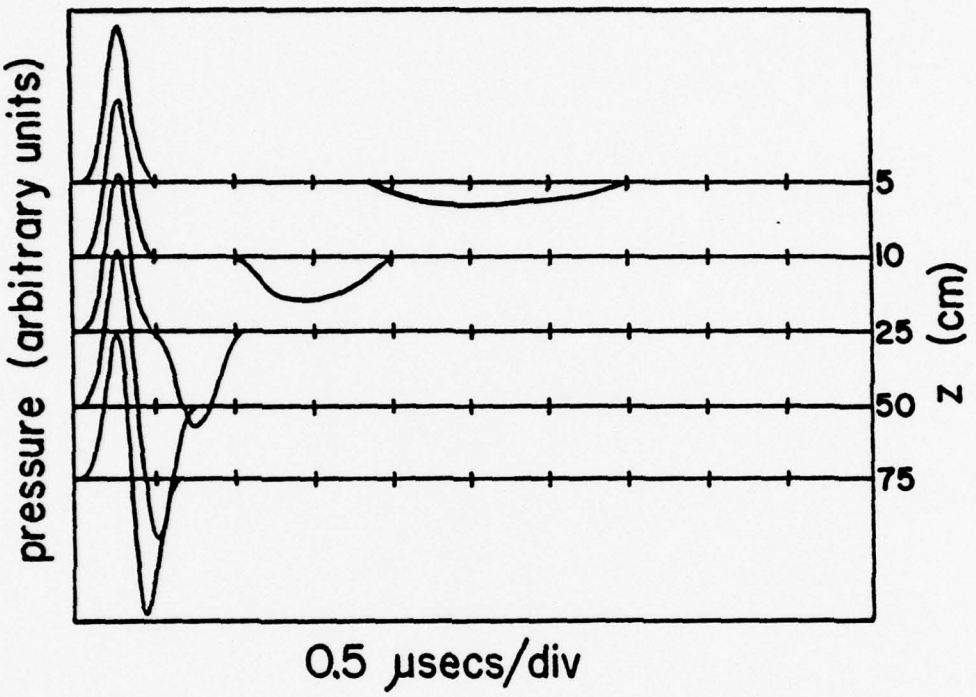

Figure 10. Calculated integrated pressure versus time curves, for a 1.91 cm radius piston source and a coaxially aligned 0.32 cm radius receiver.

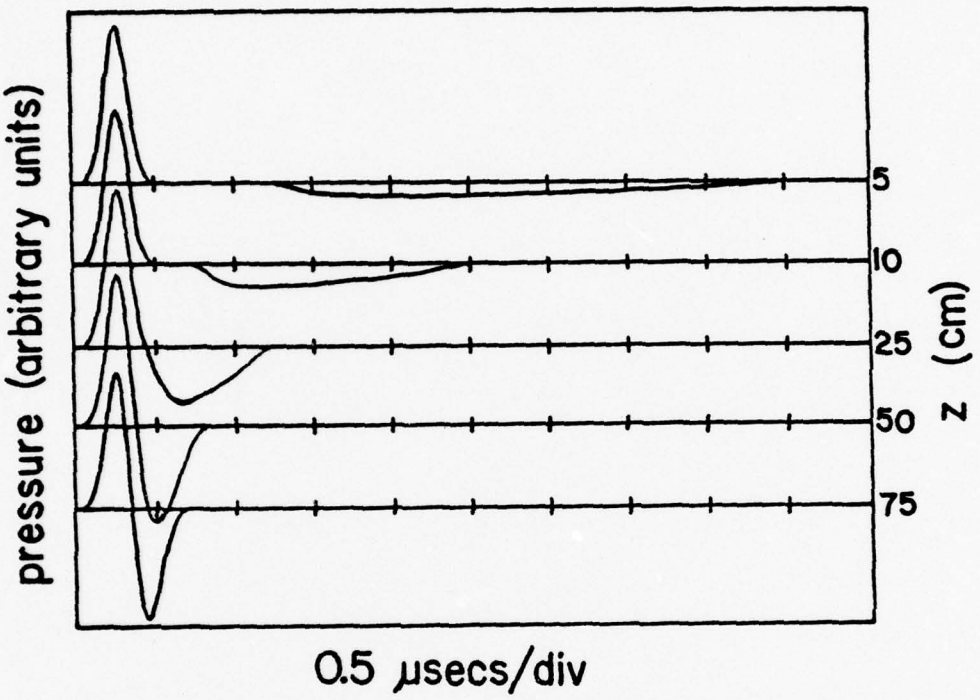

Figure 11. Calculated integrated pressure versus time curves, for a 1.91 cm radius source and a coaxially aligned 0.64 cm radius receiver.

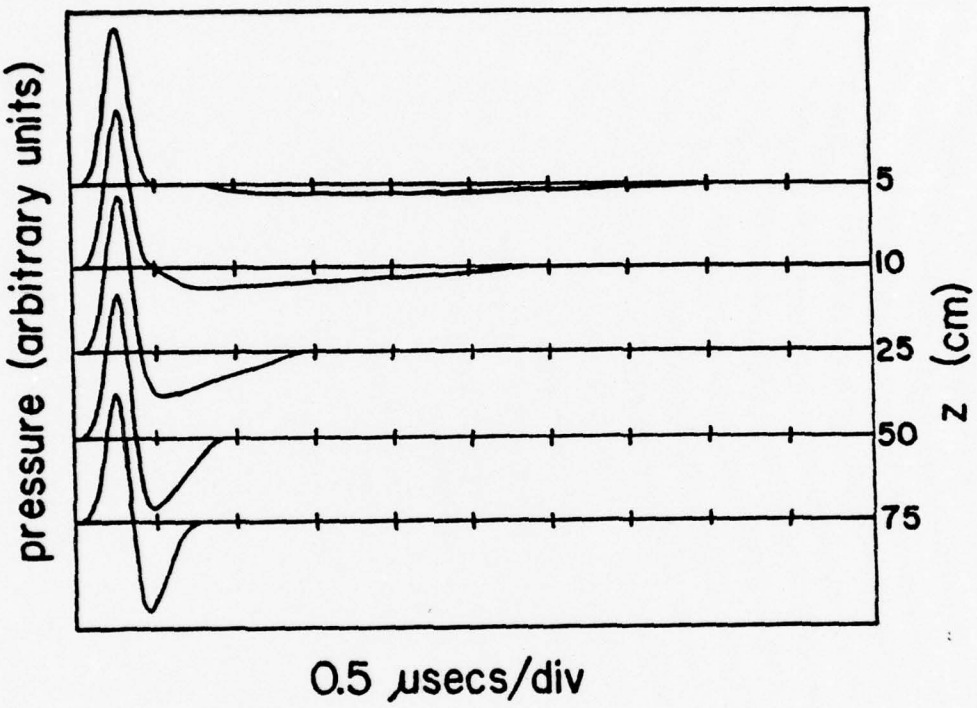

Figure 12. Calculated integrated pressure versus time curves, for a 1.91 cm radius source and a coaxially aligned 0.95 cm radius receiver.

effect of a larger receiver radius is to further broaden in time the ring source contribution. As the receiver radius becomes comparable to that of the source, the signals emanating from the source perimeter elements overlap the plane wave pulse, even for small z values, so that the resulting time variation is a positive pulse followed immediately by a broad negative tail.

IV. IMPULSE GENERATION AND DETECTION SYSTEM

To show that the above analysis does apply in practice we have made an experimental investigation of transient pressure fields using a number of source-receiver configurations. Two lead zirconate-lead titanate discs were used as sources: one of 1.91 cm radius by 2.54 cm thick, the other 3.18 cm radius by 5.08 cm thick. Each was epoxied into a brass baffle as shown in Fig 1, and the entire front surface was lapped flat to within $\pm$ .0005 in. The lapped surface was then coated with silver conductive paint, forming the ground electrode of the transducer. The source assembly was suspended in a water tank from a mounting assembly that allowed it to be translated and also rotated about two major axes.

A Cober Model 605P high voltage pulse generator together with a resistive matching network was employed to obtain the desired voltage pulse shape across the source electrodes. These pulses were nominally of 1200 volt peak amplitude, and 0.2 μsec width, and closely approximated a Gaussian. A scope trace photograph of a typical voltage pulse measured across the 1.91 cm radius source is shown in Fig 13.

One type of receiving transducer we employed were lead zirconate-

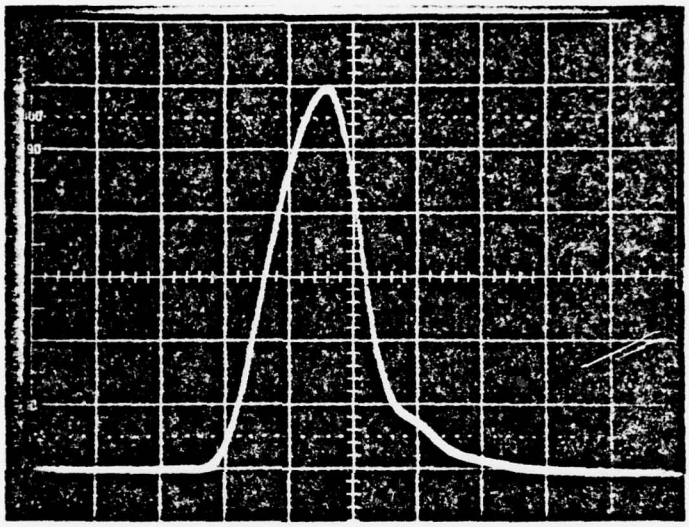

Figure 13. Oscilloscope trace of a typical voltage pulse applied to the 1.91 cm radius source transducer. The vertical sensitivity is 200 volts/div and the horizontal sweep rate is 0.1 μsec/div.

lead titanate cylinders ranging from 0.32 cm to 0.95 cm in diameter, and from 1.6 cm to 2.54 cm in thickness. Each of these was epoxied into a grounded metal cylinder and again the front surface was lapped to a flatness of $\pm$ .0005 in and coated with silver paint. This assembly formed one end of a 73 ohm coaxial line, and the other end was terminated with a 73 ohm resistor that formed the input to a wideband amplifier. Under this condition the voltage across the terminating resistor is directly proportional to the stress transient applied to the face of the transducer.[1,2] This is true only for a time interval equal to the travel time through the transducer.

The measurement system is outlined in Fig 14, with the source and receiver assemblies shown in cross-section. The receiver was supported in such a manner as to permit translations along three orthogonal axes which together with the available motions of the source made it relatively easy to keep them coaxially aligned. The receiver's output was recorded in digital form using a Biomation Model 8100 transient recorder, that sampled 2000 data points per data record at a maximum sampling rate of 10 nsec per point. The digitized data was fed directly to a PDP 11/05 minicomputer allowing for disk storage and visual display on a CRT screen.

In addition to the cylindrical receivers, a commercially available[12] probe-type receiver was employed to examine the sound field. It consisted of a small lead zirconate-lead titanate element mounted in the end of a 1.24 mm o.d. stainless steel tube. Its small size allowed us to effectively sample the pressure field at specific points. Though the damping of the element in this probe is quite high and its voltage versus pressure sensitivity fairly uniform over a wide frequency range, it did ring slightly when

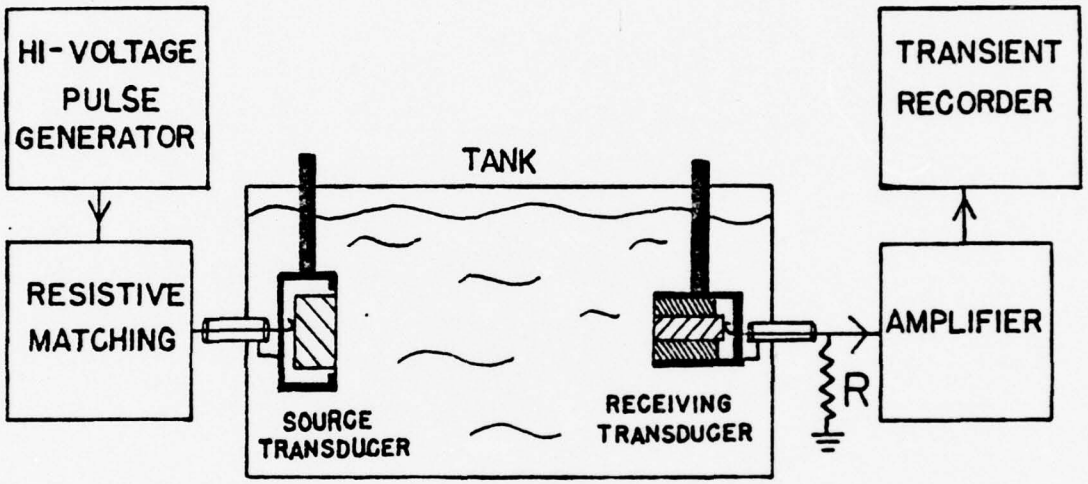

Figure 14. Sketch outlining the measurement system.

struck by the narrow impulses employed in this study. Thus care must be taken in interpreting its output. As an example consider the recordings shown in Fig 15. The upper trace is the probe output associated with a single voltage impulse applied to the source. On this relatively slow sweep rate it is possible to observe the series of pulses associated with the various internal reflections within the source. Note that these are spaced by approximately 6 μsec, the travel time between the faces of the source, and eighteen are evident on this trace. The probe output signal during the first ten microseconds after the arrival of the initial pressure impulse is shown on the lower trace in Fig 15. The initial one and one-half cycle pulse is the probe output associated with the arrival of the initial plane wave launched from the front surface of the source. A larger, opposite polarity one and one-half cycle pulse may clearly be seen to occur approximately 6 μsec later, and this is the initial pulse from the air-backed surface of the source. The other signals evident on this trace are discussed in the next section of this paper.

Not only was the probe useful in determining arrival times of various impulses but it also was used to determine the spatial uniformity of the pressure fronts. In the latter application, the probe was scanned parallel to the face of the source transducer at a separation of 10 cm. The amplitude of the initial peak of the probe output signal (see Fig 15b) was then recorded and compared with the peak value of the initial pulse calculated from Eqs. 1 and 2. Such scans of the 1.91 cm radius and 3.18 cm radius source discs are shown in Figs. 16 and 17, respectively. In these plots the experimental and theoretical peaks were normalized on the axis of the source.

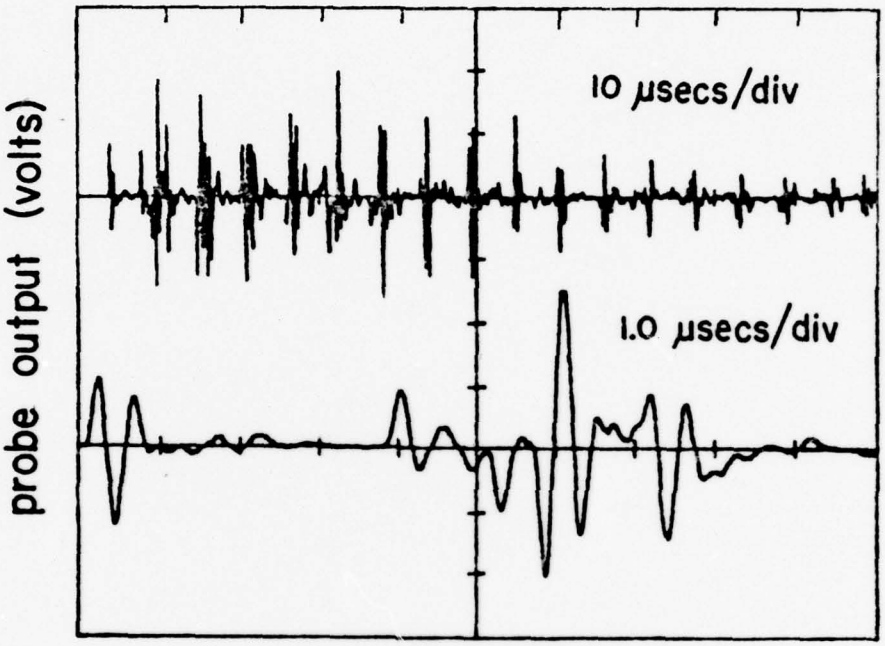

Figure 15. Oscilloscope traces of probe output voltage versus time for a single voltage impulse applied to the 1.91 cm radius source, with the probe on the source axis 2.1 cm from the source face. (a) Upper trace, 10 μsecs/div (b) Lower trace, 1 μsec/div.

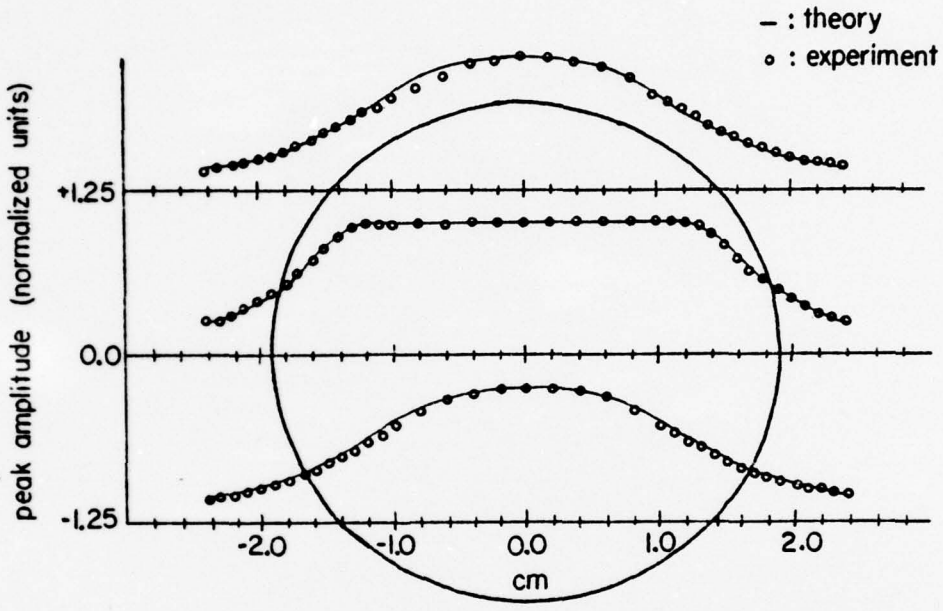

Figure 16. Comparison of the calculated initial peak pressure and the peak amplitude of the initial peak of the probe output signal along three lines in a plane parallel to the source face at a separation of 10.0 cm from the 1.91 cm radius source. Solid lines: theory; crosses: experimental values.

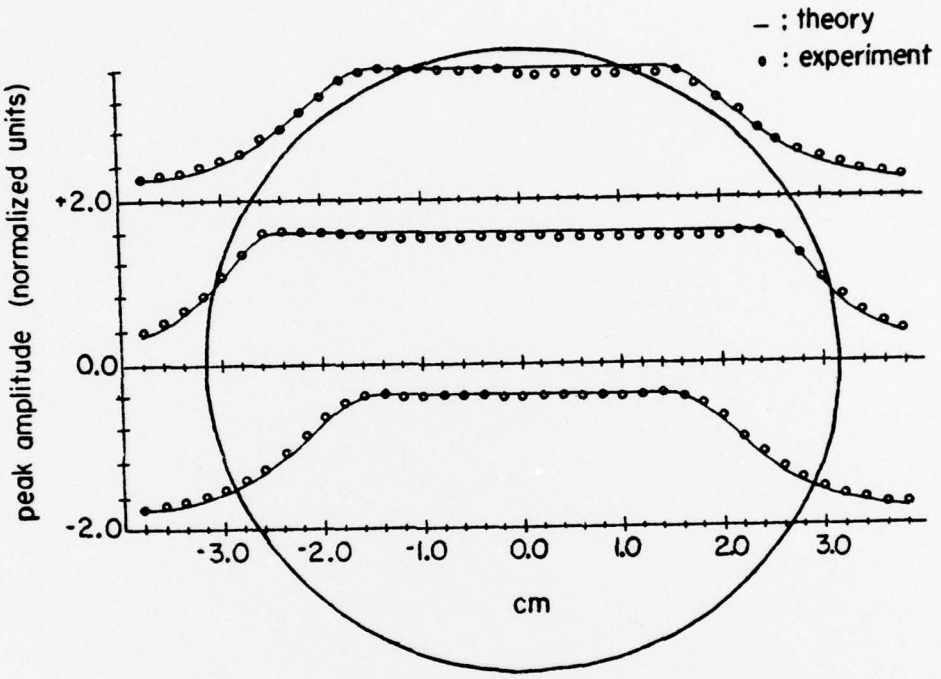

Figure 17. Comparison of the calculated initial peak pressure and the peak amplitude of the initial peak of the probe output signal along three lines in a plane parallel to the source face at a separation of 10.0 cm from the 3.18 cm radius source. Solid lines: theory; crosses: experimental values.

The probe tip was moved along straight lines parallel to the source face, one line passing through the central axis, and the others offset above and below the axis approximately two-thirds the radius of the source.

It may be seen in Figs. 16 and 17 that agreement between the experimental results and the calculation is excellent; however, special care had to be taken in mounting the discs to insure this. For example, the effect of a .015 in high spot that was present before lapping the 1.91 cm source is shown in Fig 18. The cross-hatched region in the figure indicates the high region and the effect of its presence is especially evident in the topmost experimental scan. This same transducer was also mounted in the baffle with only a .001 in epoxy-filled gap separating it from the metal baffle, which was at ground potential. Even after lapping, the received signal peaks fell off sooner than predicted, as may be seen in Fig 19. This effect is most probably due to distortion of the electric field caused by the proximity of the grounded metal baffle. With a wider epoxy gap between the transducer side surface and the metal baffle ($\sim$0.2 in) the resulting scans are those shown in Figs. 16 and 17.

V. PROBE RECEIVER DATA

It is instructive to examine in detail the output voltage signals from the probe pickup, with an emphasis on arrival times and polarities, in light of the previously discussed plane wave-ring source formulation of the impulse pressure field. The probe output was run directly into the wide-band amplifier, and then the transient recorder and minicomputer were used

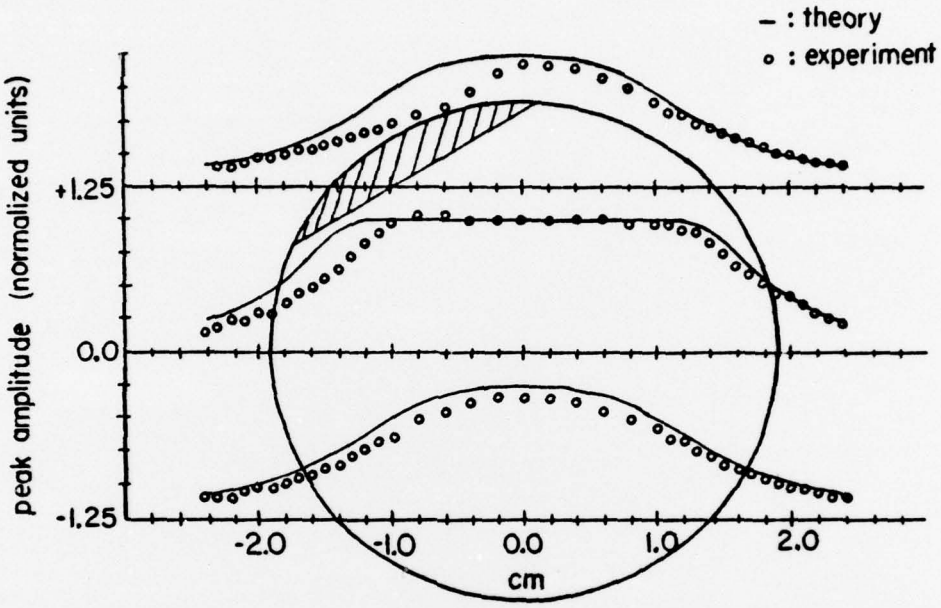

Figure 18. Comparison of the calculated initial peak pressure and the peak amplitude of the initial peak of the probe output signal along three lines in a plane parallel to the source face at a separation of 10.0 cm from the 1.91 cm radius source, indicating the effects of the presence of a high spot on the face of the source. The cross-hatched area represents this high spot.

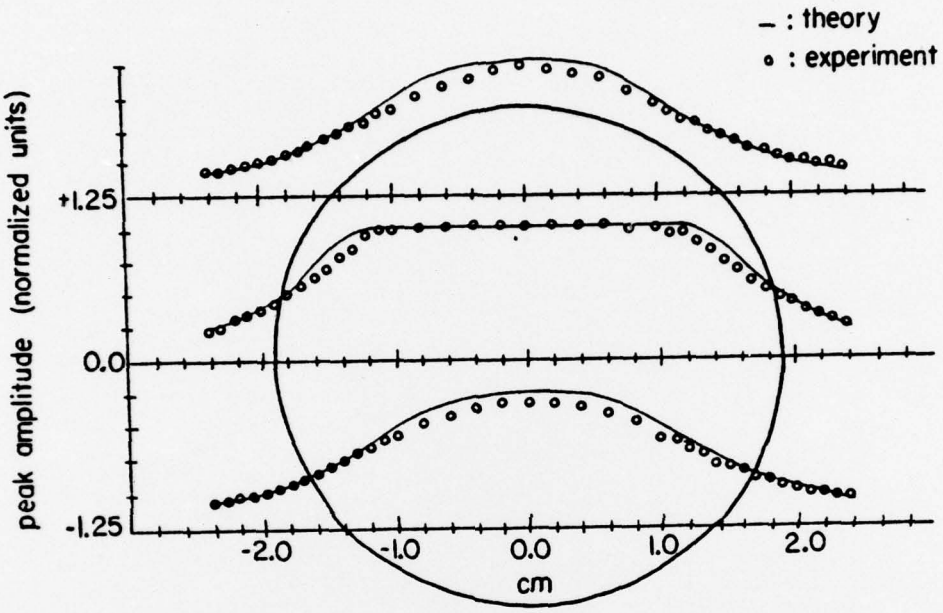

Figure 19. Comparison of the calculated initial peak pressure and the peak amplitude of the initial peak of the probe output signal, along three lines in a plane parallel to the source face at a separation of 10.0 cm from the 1.91 cm radius source, indicating the effects of a .001 in gap between the transducer side and the metal baffle.

in the manner described above to collect the data records. Returning to Fig 15a, it is only the first 10 μsec of the signal following the arrival of the initial plane wave pulse that is of interest, since the multiply-reflected signals from inside the source complicate effects that occur at later times. This portion of the signal is shown at a faster sampling rate in Fig 15b. As already mentioned the first pulse is due to the initial plane wave launched into the water, with successive pulses every 5.8 μsecs from front and rear reflections in the source. Since this trace was recorded with the probe situated on axis 2.1 cm from the source, a delay of 5 μsecs should exist between the plane wave pulse and the ring source pulse, and in fact a pulse of opposite polarity to the initial signal may be seen to be present at this time.

However, another pulse of the same polarity as the initial plane wave pulse is seen to precede the ring source signal. This pulse also was observed when the 3.18 cm radius source was used. We believe that such pulses are caused by a wave that propagates along the disc surface, originating at the perimeter, and radiating out into the water as it propagates. Travel time measurements indicate a velocity of approximately 4.0×10^5 cm/sec for this wave, an acceptable value for a surface wave on the transducer material.

The amplitudes of the ring source signal as well as the spurious surface wave one depended strongly on how well centered the probe was on the source axis. This indicates that both of these waves originate at the source perimeter. The effect of a slight displacement of the probe away from the axis is indicated in Fig 20, where signals obtained using the 3.18 cm radius by 5.08 cm thick source are shown. In this case signals from the air backed

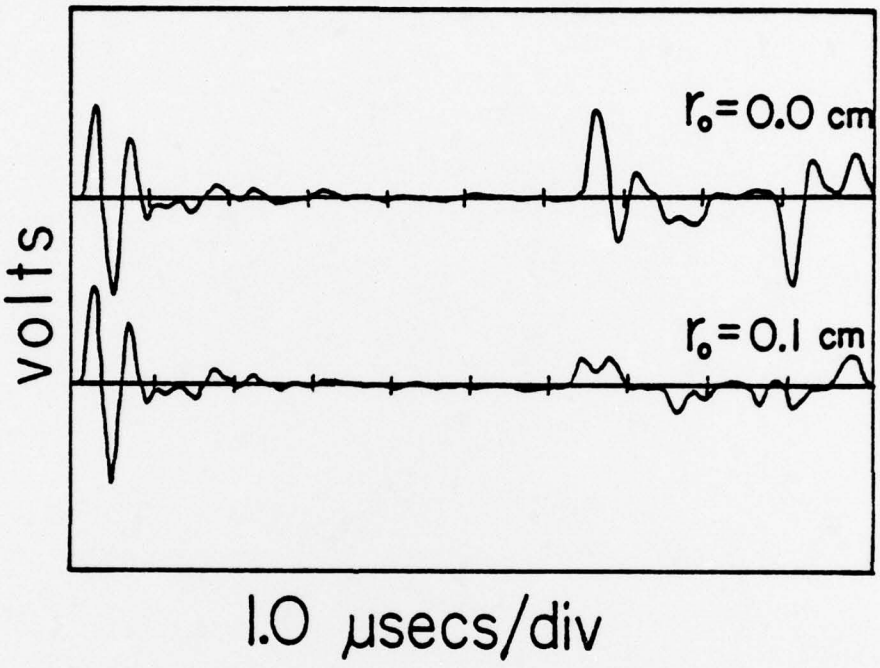

Figure 20. Oscilloscope traces of probe output voltage versus time, using the 3.18 cm radius source, at a separation of 3.4 cm. (a) Upper trace: probe tip centered on the axis; (b) Lower trace: probe tip offset 0.1 cm from the axis.

face of the transducer are delayed by 13 μsec from the initial plane wave signal. The distance from the source face was 3.4 cm and as expected the opposite polarity ring source occurs at about 8.5 μsecs after the initial pulse. Again note the presence of the earlier pulse that we have attributed to surface wave excitation along the periphery. The upper trace was obtained with the probe on axis. The lower trace shows the received signal when the probe was offset 1 mm from the source axis. In this case both delayed pulses are broader in time as well as lower in amplitude than when the probe was centered on the axis.

As z increases, the ring source pulse approaches the plane wave pulse more rapidly than the pulse attributed to a surface mode, and eventually these overlap. This is apparent in Fig 21, which shows a series of probe signals for various z distances, the plane wave pulse arrival marking the beginning of each curve. On the uppermost trace, recorded at z = 3.5 cm, three pulses can be distinguished in the receiver output: that due to the plane wave's arrival, which marks the start of the curve; another pulse of the same polarity as the plane wave, delayed 6.3 μsecs from the plane wave pulse; and finally a pulse of opposite polarity to the plane wave, delayed 8.4 μsecs from it. As the separation between the source and receiver is increased, the third pulse approaches the plane wave pulse more rapidly than the second so that these delayed pulses eventually begin to overlap as seen in Fig 21 for a separation of 4.5 cm. Since the probe's response peaks at 2.5 Mhz, its amplified output actually overdrives the recorder input when the two delayed pulses are time separated such that this resonance condition is enhanced as is evident for the trace recorded at a separation of 6.5 cm. As

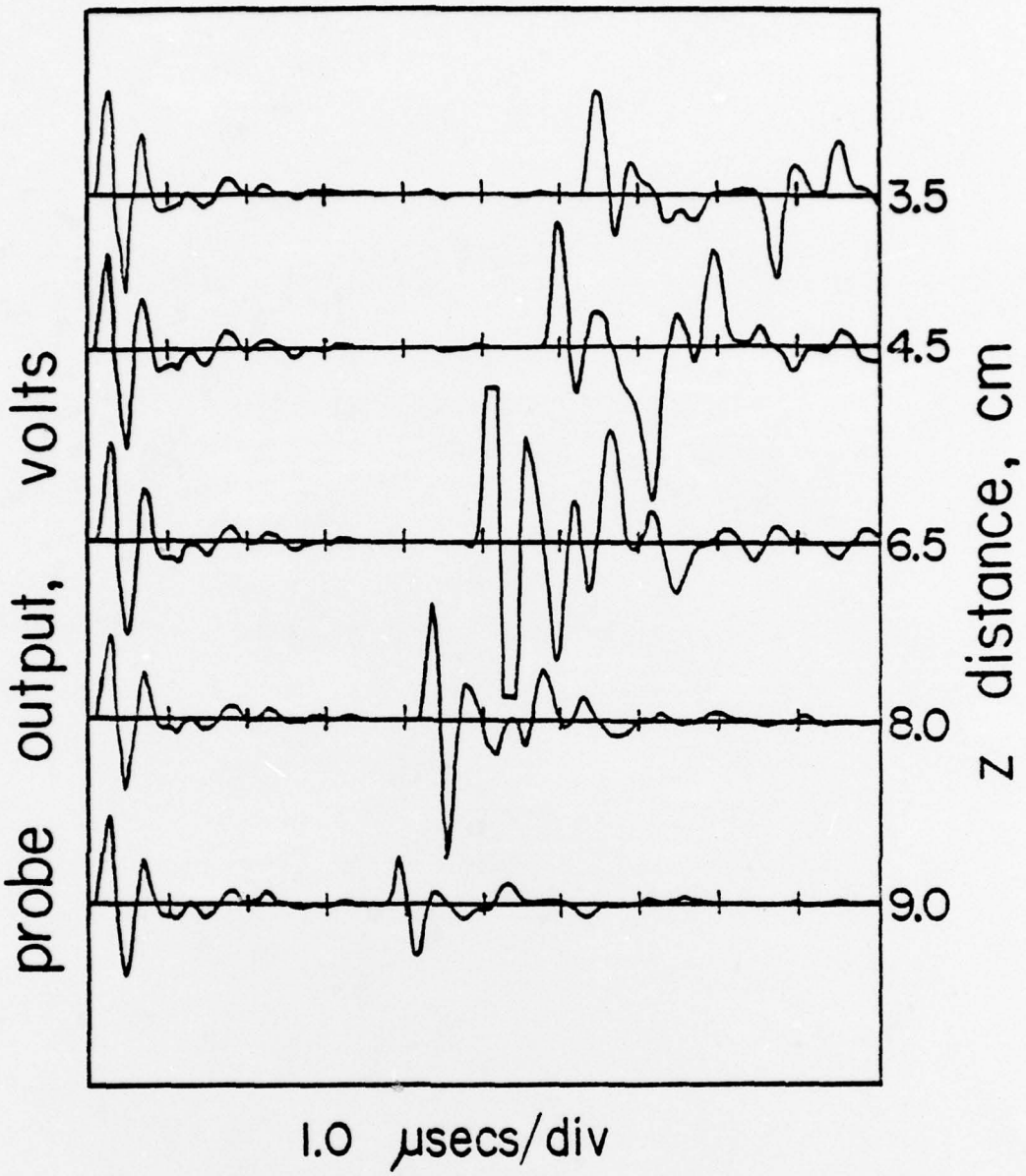

Figure 21. Oscilloscope traces of probe output voltage versus time, for the probe centered on the axis of the 3.18 cm radius source, at various z values.

the separation is further increased beyond this, the two trailing pulses overlap to a greater extent, reducing the amplitude of the delayed output pulse. Note that the plane wave pulse is effectively unchanged during this change of position.

VI. CYLINDRICAL RECEIVER DATA

The acoustic field was also examined using the finite diameter cylindrical receivers, which for the measurements were always aligned coaxially with the source transducer. A set of received signals taken at five different z values is shown in Fig 22 for the 1.91 cm radius source and a 0.32 cm radius receiver. At z = 5 cm the plane wave signal is clearly distinct from any other signals; however, a fairly large amplitude signal of the same polarity can be seen to occur about 2 usecs after the plane wave. This delayed signal is attributed to interaction between the ring source wave, and radiation from the surface wave discussed above. This effect was encountered at small z values with all the receiving rods used. Excepting this difference, there is very good agreement between the experimental results shown in Fig 22 and the calculated profiles shown in Fig 10. Additional data is shown in Figs. 23 and 24 for 0.64 cm radius and 0.95 cm radius receivers, respectively, using the same source transducer and driving pulse. Again, the reversal of polarity at small z values is evident for small source-receiver separations, but in general the agreement between the experimental results and the calculations is good. As can be seen in Figs 23 and 24, the plane wave pulse remains unchanged while the ring source signal

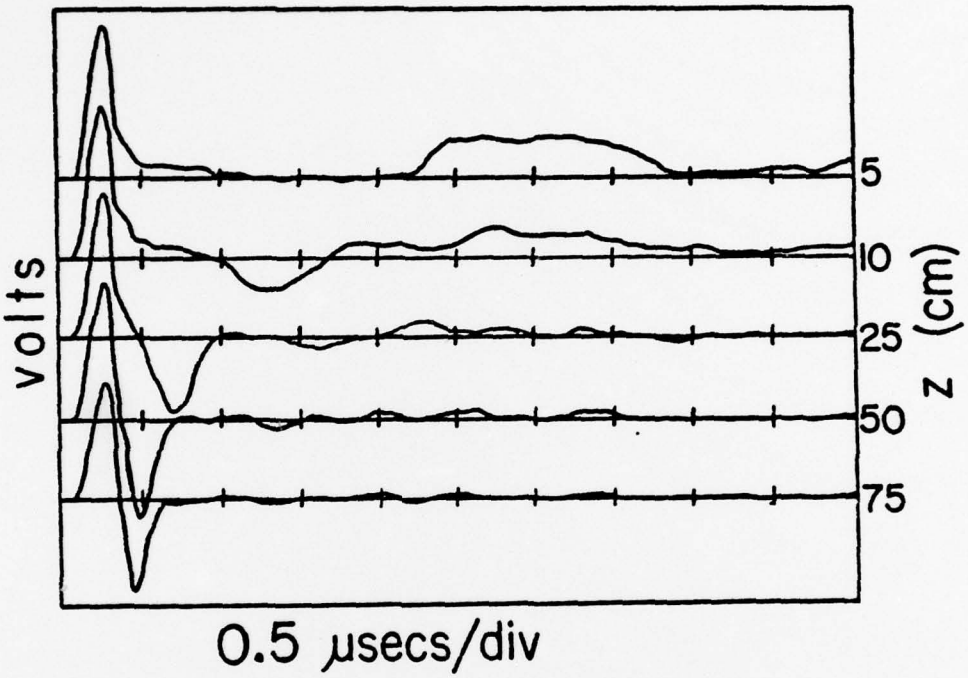

Figure 22. Received signal using the 1.91 cm radius source and a 0.32 cm radius cylindrical receiver, centered on the source axis, at five different z separations. The beginning of each curve is marked by the plane wave arrival.

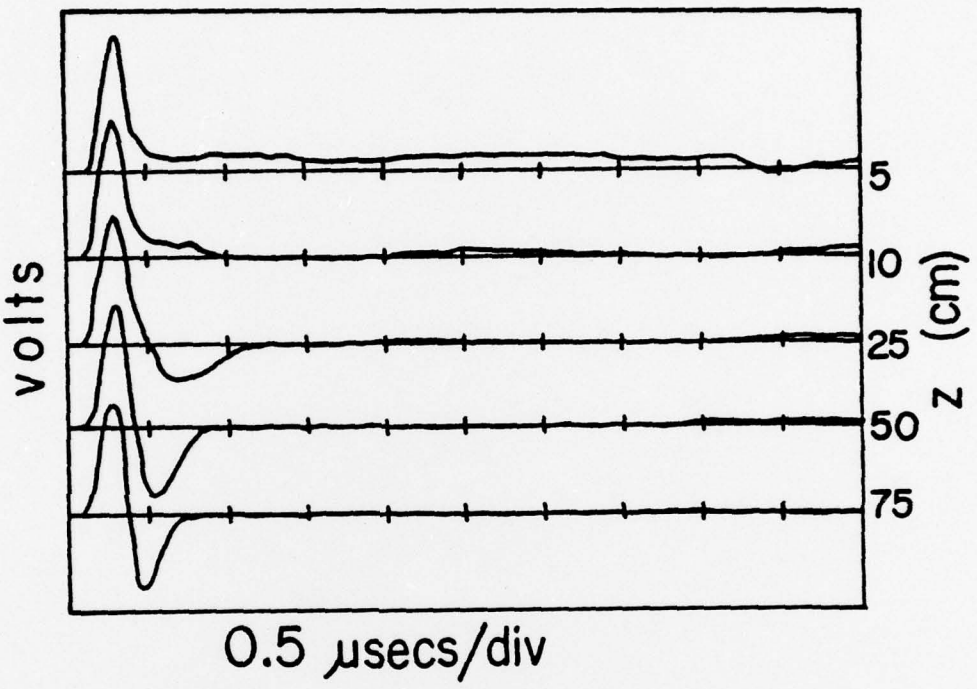

Figure 23. Received signals using the 1.91 cm radius source and a 0.64 cm radius cylindrical receiver, centered on the source axis, at five different z separations. The beginning of each curve is marked by the plane wave arrival.

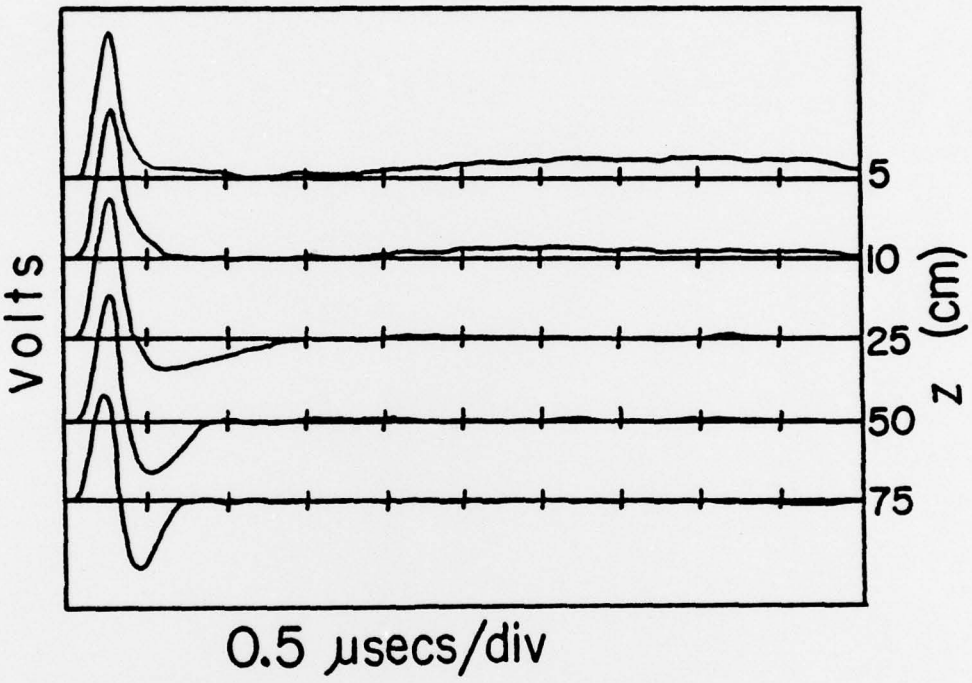

Figure 24. Received signals using the 1.91 cm radius source and a 0.95 cm radius cylindrical receiver, centeres on the source axis, at five different z separations. The beginning of each curve is marked by the plane wave arrival.

becomes compressed in time and approaches more closely the plane wave pulse as the separation increases. The relative amplitude of the ring source signal is somewhat lower than expected, most likely due to the fact that the ring source front is never incident normal to the receiver face.

VII. SUMMARY

We have made calculations of the transient pressure field in an ideal fluid generated by a baffled circular piston source assuming that the velocity of the piston face is a Gaussian impulse. As indicated by other authors, at any point in the fluid the resultant pressure field may be represented simply as the sum of two waves. For points within the periphery of the source these consist of a plane wave and a second wave effectively radiated from a ring source defined by the piston perimeter. We have also conducted an experimental study of the transient fields of thick circular transducers. These were driven by unipolar voltage impulses and the radiated fields were examined using various types of receiving transducers. We found good agreement between the results of our calculations and our experimental data for the source-receiver configurations used in our studies. Our results emphasize that care must be taken in interpreting the results of transient-type experimental acoustic phenomena.

ACKNOWLEDGEMENTS

The authors wish to thank T. R. Hickman and L. A. Burns for their technical assistance. This research has been supported in part by the Office of Naval Research.

REFERENCES

+ Present address: Naval Research Laboratory, Washington, D.C.

1. M. Redwood, J. Acoust. Soc. Am. 33, 527-536 (1961).
2. E. F. Carome, P. E. Parks, and S. J. Mraz, J. Acoust. Soc. Am. 36, 946-952 (1964).
3. E. F. Carome, P. A. Fleury, and W. J. Wagner, J. Acoust. Soc. Am. 36, 2368-2373 (1964).
4. R. A. Graham, F. W. Neilson, and W. B. Benedick, J. Appl. Phys. 36, 1775-1783 (1965).
5. P. R. Stepanishen, J. Acoust. Soc. Am. 49, 1629-1683 (1970).
6. M. P. Felix, J. Acoust. Soc. Am. 58, 626-629 (1975).
7. M. R. Layton and E. F. Carome, J. Acoust. Soc. Am. 61, S14 (A) (1977).
8. E. F. Carome, C. E. Moeller, and N. A. Clark, J. Acoust. Soc. Am. 40, 1462-1466 (1966).
9. O. G. Kozina and G. I. Makarov, Soviet Phys. Acoust. 7, 39-43 (1961).
10. B. Rossi, Optics (Addison-Wesley, Reading, MA, 1959) 2nd ed., pp. 18-31.
11. P. M. Morse and K. U. Ingard, Theoretical Acoustics, (McGraw-Hill, New York, 1968) p. 375.
12. Marketed as the Mediscan Ultrasonic Microprobe by Mediscan, Inc., 544 Tolland St., E. Hartford, CONN. 06108.